# INVESTIGATING THE IMPACTS OF INCLUDED ANGLES ON FLOW AND HEAT TRANSFER IN CROSS-CORRUGATED TRIANGULAR DUCTS WITH FIELD SYNERGY PRINCIPLE

*Zuoyi CHEN* [1,2*], *Lizhi ZHANG* [2], *Han SONG* [3]

[1] Guangdong University of Education, Guangzhou, 510303, China, chenzuoyi@gdei.edu.cn
[2] Key Laboratory of Enhanced Heat Transfer & Energy Conservation of the Ministry of Education, South China University of Technology, Guangzhou, 510640, China
[3] School of Sustainable Development of Society and Technology, Mälardalen University, 72123, Sweden

***Abstract:*** *Included angles ($\alpha$) have vital effect on the flow and heat transfer in cross-corrugated triangular ducts. The friction factor and Nusselt number were estimated at different Reynolds numbers from both experiments and simulations. Results show that the flow in the duck with $\alpha$=90 has the largest friction factor and Nusselt number. However, the included angle influences the flow and heat transfer in cross-corrugated triangular ducts in different ways. The field synergy principle was used to explore the mechanism of the different impacts of the included angle. Results show that the flow in the cross-corrugated triangular duct with $\alpha=90^o$ has the smallest domain averaged included angle ($\beta_m$), which implies the best synergy performance. The results of the field synergy principle were also validated by analyzing the performance evaluation criterion and studying the velocity vector and temperature distributions.*

***Key Words:*** *cross corrugated triangular channel, included angle, field synergy principle*

## 1 Introduction

Cross-corrugated channel is the basic channel geometry in plate heat exchangers and are encountered in many industrial areas such as electronic cooling, spacecraft, air conditioning, refrigeration, automobiles, aircrafts, ships, and so on. The benefits of such geometries are that they have efficient heat exchange capabilities and strong mechanical strength, even with very thin material wall thickness [1-5].

A schematic of cross-corrugated triangular ducts is shown in Figure 1. Flat plates are corrugated to form a series of parallel equilateral triangular ducts. Sheets of the corrugated plates are then stacked together to form a $90^o$ orientation angle between the neighboring plates, which guarantees the same flow pattern for both fluids.

Literature review shows that most of efforts have been focused on the cross corrugated ducts with sinusoidal cross section, except our previous studies [3-6] that investigate the fluid flow and heat transfer in the cross corrugated ducts with triangular cross section. The simulated results show very complex flow patterns due to the generated fluid recirculation or swirl flows. Obviously, the included angles have significant influences on the fluid flow and, further, heat transfer. This paper studied the influences of the included angles based on field synergy principle [7,8]. Experimental measurements were also conducted to verify the simulation results. This work gives insights and guidelines to the design and applications of the cross corrugated ducts with triangular cross section.

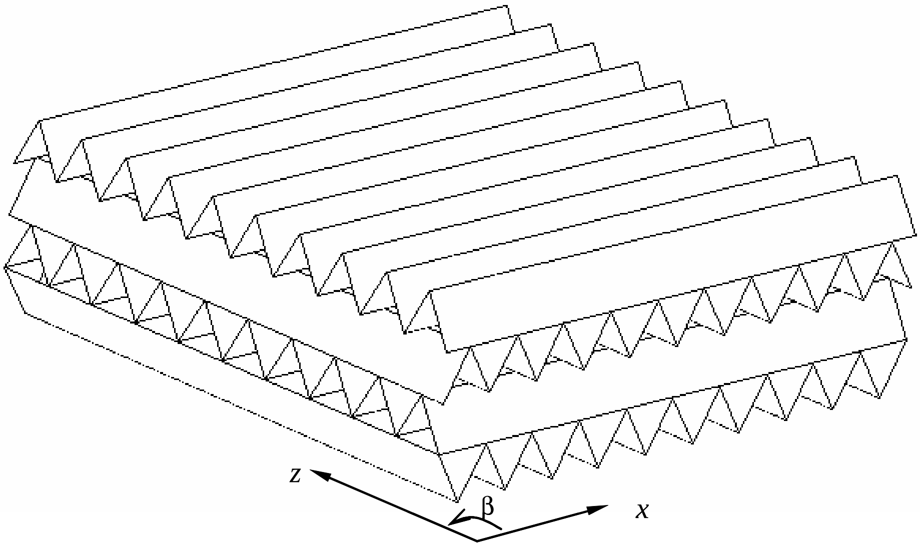


**Fig.1. Flow channel geometry**

## 2 Mathematic models

### *2.1 Governing equations [9]*

The general form of the mass continuity equation as shown below is valid for compressible and incompressible flows:

$$\frac{\partial \rho}{\partial t} + \frac{\partial}{\partial x_i}(\rho u_i) = 0 \tag{1}$$

where ρ is the fluid density (kg/m$^3$), $t$ the time (s), $u$ the flow velocity (m/s), subscript $i$ denotes coordinates directions.

The conservation of momentum in the $i$th direction in an inertial reference frame is governed by:

$$\frac{\partial}{\partial t}(\rho u_i) + \frac{\partial}{\partial x_j}(\rho u_i u_j) = \frac{\partial \sigma_{ij}}{\partial x_j} + B_i \tag{2}$$

where $B_i$ is a body force in the $i$th direction. It includes contributions from gravitational acceleration and external body forces. The stress tensor, $\sigma_{ij}$, is given by:

$$\sigma_{ij} = -p\delta_{ij} + \mu\left[\frac{\partial u_i}{\partial x_j} + \frac{\partial u_j}{\partial x_i}\right] - \frac{2}{3}\mu\frac{\partial u_k}{\partial x_k}\delta_{ij} \tag{3}$$

where the final term is the effect of volume dilation (zero for an incompressible fluid). The pressure and molecular viscosity are denoted by $p$ (Pa) and $\mu$ ($Ns/m^2$), respectively; $\delta_{ij}$ is the Kroneker operator, which equals to 1 when $i=j$, and 0 when $i\neq j$.

In addition, a general scalar advection-diffusion equation for a dependent variable, $\phi$, is given by:

$$\frac{\partial(\rho\phi)}{\partial t} + \frac{\partial}{\partial x_i}\left[\rho u_i\phi - \Gamma\frac{\partial\phi}{\partial x_i}\right] = S \tag{4}$$

$\Gamma$ is the diffusion coefficient and $S$ a source or sink term representing creation or destruction of $\Gamma$.

For fully compressible flow, the energy transport equation is solved for the total enthalpy, $H$, according to:

$$\frac{\partial(\rho H)}{\partial t} + \frac{\partial}{\partial x_i}\left[\rho u_i H - \lambda\frac{\partial T}{\partial x_i}\right] = \frac{\partial\rho}{\partial t} \tag{5}$$

where $\lambda$ is the thermal conductivity [kW/(mK)] and $T$ the temperature (K). $H$ is expressed in terms of the static enthalpy, $h$, according to:

$$H = h + \frac{1}{2}u^2 \tag{6}$$

$$h = U_{ie} + \frac{p}{\rho} \tag{7}$$

For weakly compressible and incompressible flow, the kinetic energy term ($1/2\rho u^2$) is assumed to be negligible compared to the internal term, $U_{ie}$. The pressure work term, $p/\rho$, may also be safely ignored.

The above equations (Equ. 1-7), also known as the Navier-Stokes equations, represent five transport equations in the seven unknown field variables $u_x$, $u_y$, $u_z$, $p$, $\rho$, $h$, and $T$. The thermal equation of state provides a sixth equation relating density, $\rho$, to temperature $T$ and pressure $p$. For air, this equation is called the idea gas equation. The seventh equation required to close the entire system is a thermodynamic relation between the state variables. For air, this equation defines the function of static enthalpy in terms of temperature and pressure, i.e., $h=h(T,P)$. Since the fluid is assumed to be thermally perfect, the static enthalpy is a function of temperature only.

### *2.2 Methodology*

A commercial computational fluid dynamics (CFD) software Fluent [10] was used to simulate the flow and heat transfer in cross corrugated triangular ducts. The governing equations were solved by using standard finite difference methods that employ control-volume based discretization techniques along with a pressure-correction algorithm. The N-S equations (Equ. 1-7) were solved by SIMPLEC scheme, while the convective term and the diffusive term in the energy equation were solved by first-order upwind implicit approximation and second-order central difference scheme respectively.

The meshes on the outside walls of a computational block are shown in Fig.2. The graph depicts the meshes only for the first 3 and a half cycles, to get an amplified view of the mesh structure. Totally there are 10 cycles in this block. Boundary conditions are defined. A uniform temperature and non-slip velocity wall conditions are assumed. At the inlet, velocity is set to uniform and parallel to the corrugation of the upper wall.

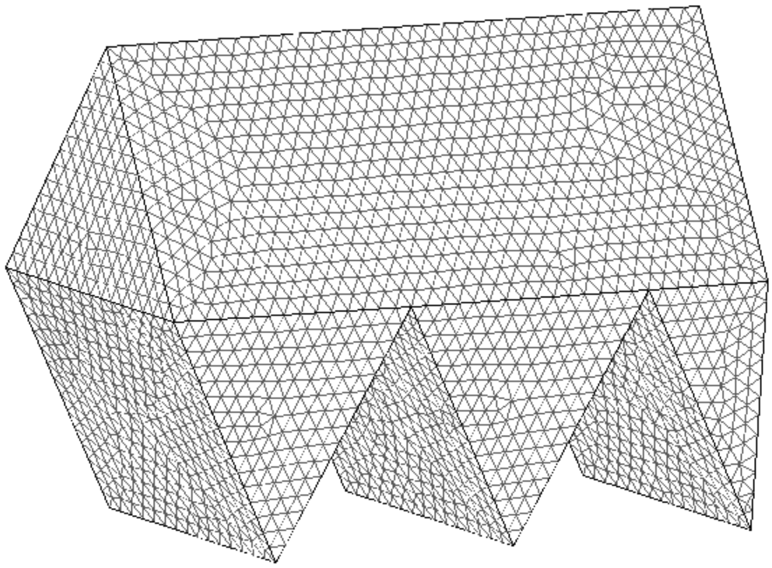

**Figure 2 External mesh on the plate surfaces**

## 3 Experiment setup

A test rig, as shown in Fig. 3, was used to perform heat transfer and pressure drop experiments. It is an open circuit system comprising of five main components: a variable speed blower, a wind tunnel, an upstream section, a test section, and a down-stream section. Air conditioned indoor air is supplied to the tunnel by a variable speed blower. The volumetric air flow rates can be adjusted to have different Re numbers from 50 to 30,000. The low speed wind tunnel is to ensure a continuous, steady air supply. The volumetric air flow rates are measured by a set of nozzles in the wind tunnel. In the upstream and down-stream sections, wind screens are installed in the duct to have steady and uniform air flow to the heat exchanger. In the test section, a heat exchanger in the form of cross-corrugated triangular duct is flanged between the upstream and the down-stream sections. The maximum air velocity to the test section is 30 m/s, with centerline turbulence intensity level less than 0.35%. The ducting work is made of high-precision smooth acrylic-glass tubes. In the upstream section, the pipe length to diameter is L/D = 187.5. The different sections are connected by custom-designed couplings. The whole ducting work is insulated with 10mm thick fiber glass.

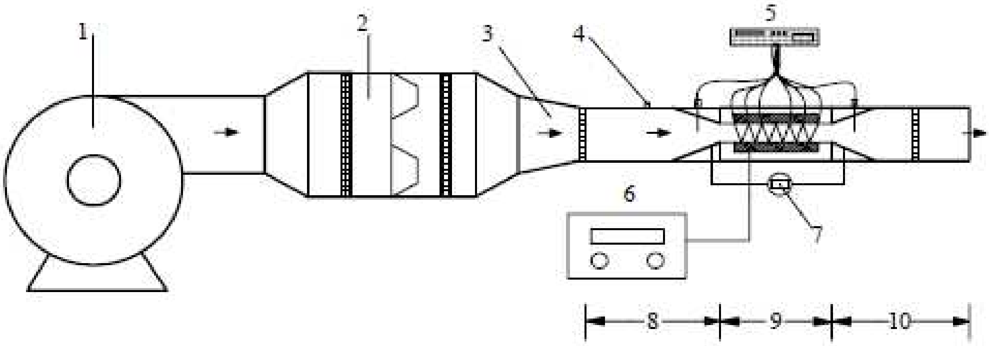

1) blower, 2) straightener, 3) reducing pipe, 4) velocity measurement section 5) data acquisition device, 6) direct-current main, 7) manometer, 8) entrance section, 9) experimental section, 10) exit section

**Figure 3 System sketch of experimental setup**

According to the defined boundary conditions, a uniform temperature was required at the wall surface. However, with the geometry shown in Figure 1, it is difficult to realize uniform wall temperature or constant wall heat flux during experimental tests. In order to overcome the difficulties, triangle troughs were etched on two copper plates, which sizes are 160*160*7mm. The number of trough is 15. The duct wall thickness at apex angle is 2mm. Then one of the two plates was reversed and vertically overlapped with the other, as shown in Figure 2. Comparing the geometries shown in Figure 1 and 2, they have the same channel structures, except the wall. The geometry shown in Figure 3 was used in all of the tests with different included angles ($\alpha$ = 45°, 60°, 90° and 120°).

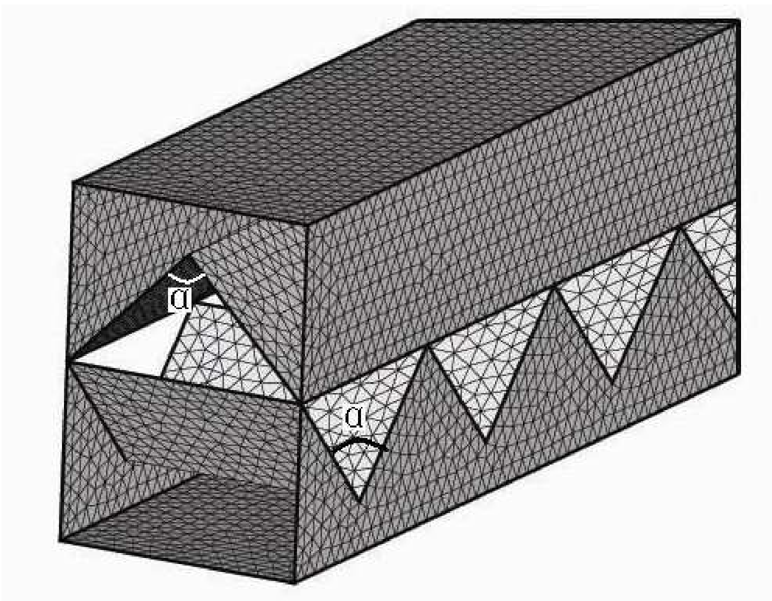


**Fig4 Peripheral structure of geometry**

Thermal couples, type K and 1.5mm in diameter, were attached to the inner surface to measure the temperature. The measured temperatures are then averaged transversely across y-axis to have the transversely local mean temperatures along the duct. On the outer surfaces of the copper plates, uniform heating is provided by means of electrically heated nichrome heater wire (0.5mm thick) which is wounded uniformly around the external surface of the exchanger. Due to the excellent heating efficiency (99%) of the nichrome heater wire, nearly all the electric power supplied can be converted to heating power. The electric power supplied to the heater can be adjusted from 50 to 1000W via a variable transformer and monitored by a multimeter throughout every experiment. The entire exchanger assembly is thermally insulated from its ambient environment by a 10mm thick silica aerogel foam. The exchanger plate has a very thin wall thickness of 1 mm, which is used to minimize the thermal resistance through the duct wall to achieve high heat transfer from the heater wire, which is attached on the outer surface, to the inner surface of the exchanger.

On fluid side, six thermal couples are installed before and after the exchanger to measure the fluid inlet and outlet temperatures. The six signals are averaged to get the mean values for inlet and outlet temperatures. Pressure drop across the exchanger is also measured by a digital pressure drop gauge (DP-1000III), reading to 0.1 Pa. Anemometers (Testo-311) are used to measure the mean velocities to and from the exchanger. Thus the air flow rates through the duct can be calculated and are checked with the measured values from wind tunnel nozzles. The differences between nozzle measured and anemometers measured are controlled to within 1%.

## 4 Experimental results

The measured fluid velocity, pressure and temperature were used to calculate cycle friction factors and Nusselt numbers.

The cycle-average friction factor is calculated by:

$$f_{\mathrm{m}} = \frac{\frac{p_{\mathrm{i}} - p_{\mathrm{o}}}{L_{\mathrm{cyc}}} D_{\mathrm{h}}}{\frac{1}{2}\rho u_{\mathrm{m}}^{2}} \tag{8}$$

where $L_{cyc}$ is the length of a cycle, (m); $p_i$ and $p_o$ are pressure at inlet and outlet of a cycle, respectively, (Pa). $u_m$ is the area-weighted mean velocity through a cross-section, (m/s), which is calculated as:

$$\mathrm{u}_{m} = \frac{\int u_{x} A_{x} dx}{V_{cyc} / L_{cyc}} \tag{9}$$

$D_h$ is the hydraulic diameter of the channel, which is defined as:

$$D_{\mathrm{h}} = \frac{4V_{\mathrm{cyc}}}{A_{\mathrm{cyc}}} \tag{10}$$

where $V_{\mathrm{cyc}}$ and $A_{\mathrm{cyc}}$ are the volume and the surface area of the channel, respectively.

The cycle-average Nusselt number, $Nu_m$, is defined as:

$$Nu_{\mathrm{m}} = \frac{h_{\mathrm{m}} D_{\mathrm{h}}}{\mathrm{k}} \tag{11}$$

where $h_m$ is the cycle-average heat transfer coefficient and $k$ is the thermal conductivity. $h_m$ is evaluated from the temperature difference between the inlet and the outlet of a cycle:

$$h_{\mathrm{m}} = \frac{\rho u_{\mathrm{m}} c_{\mathrm{p}} A_{\mathrm{ci}} \left(T_{\mathrm{i}} - T_{\mathrm{o}}\right)}{A_{\mathrm{cyc}} \Delta T} \tag{12}$$

where $c_p$ is the specific heat of fluid, kJ/(kgK); $A_{ci}$ is the cross-sectional area at inlet or outlet of a cycle, ($m^2$); $T_i$ and $T_o$ are fluid temperature at inlet and outlet of a cycle, respectively (K); $\Delta T$ is the logarithmic temperature difference between the wall and the fluid, which is calculated by:

$$\Delta T = \frac{(T_{\mathrm{i}} - T_{\mathrm{w}}) - (T_{\mathrm{o}} - T_{\mathrm{w}})}{\ln \dfrac{T_{\mathrm{i}} - T_{\mathrm{w}}}{T_{\mathrm{o}} - T_{\mathrm{w}}}} \tag{13}$$

where $T_w$ is the wall temperature (K).

Experiments were conducted firstly for the cross-corrugated triangular ducts with an included angle of 90°. The mean friction factors and mean Nusselt numbers were evaluated at different Reynolds numbers, which are calculated as:

$$\mathrm{Re} = \frac{\rho u_{\mathrm{m}} D_{\mathrm{h}}}{\mu} \tag{14}$$

where ρ is fluid density and μ is fluid molecular viscosity. Results are shown in Figure 5.

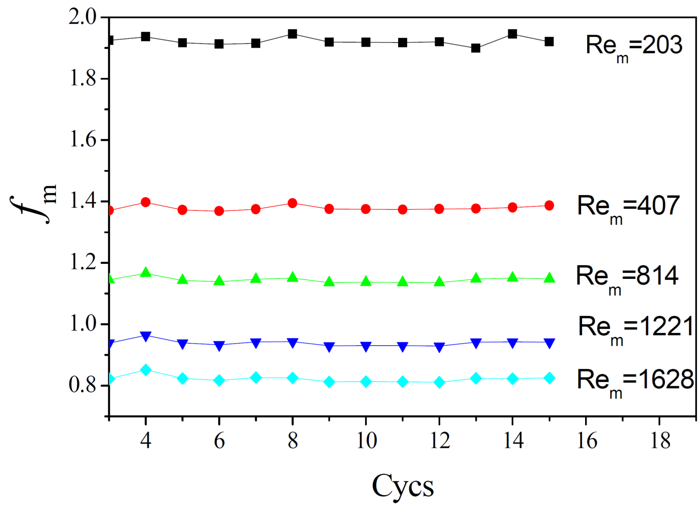


(a) $f_m$

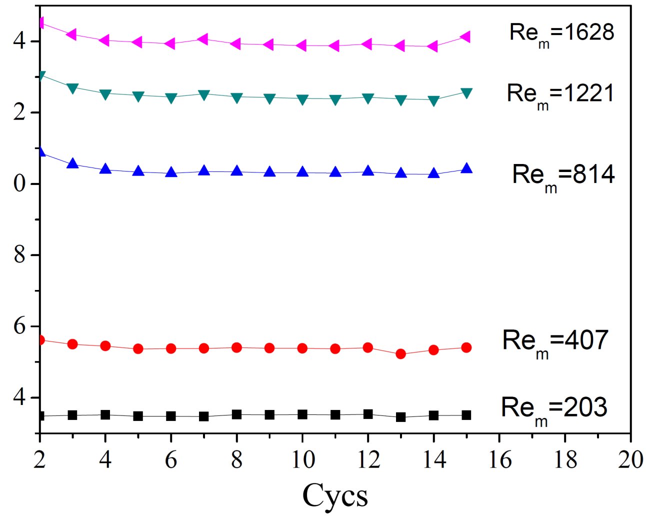


(b) $Nu_m$

**Figure 5 $f_m$ and $Nu_m$ of each cycle for ducts with included angle $\alpha$=90°**

It is quite clear that the values of channel $f_m$ and $Nu_m$ are quite stable except in the 2 or 3 channels at the inlet and 1 or 2 channels at the outlet. Here, the stabilized values were considered as fully developed mean friction factor ($f_D$) and fully developed mean Nusselt number ($Nu_D$).

In order to study the impacts of included angles on flow and heat transfer, the same procedures were conducted for cross-corrugated triangular ducts with different included angles. The fully developed mean friction factor and fully developed mean Nusselt number were evaluated at various included angles and $Re_m$. Results were illustrated by scatters in Fig 6. In the meantime, $f_D$ and $Nu_D$ were also simulated based on the previously described model. The predicted values were presented by the curves in Fig 6. In general, the simulated results agree with the results obtained from measured parameters.

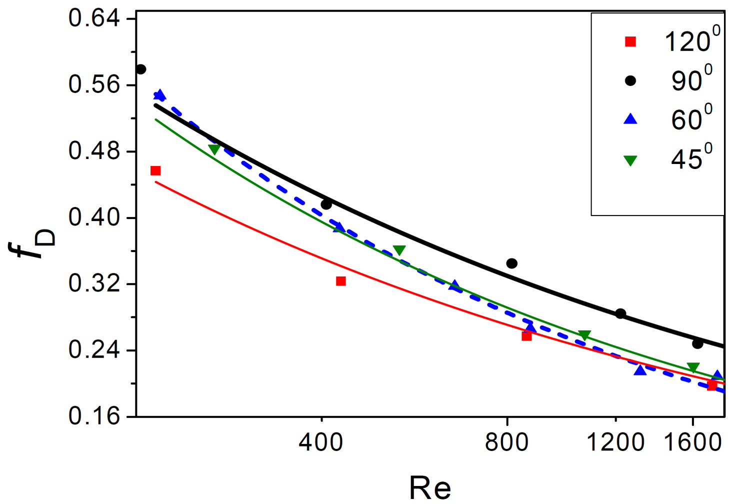


(a) $f_D$

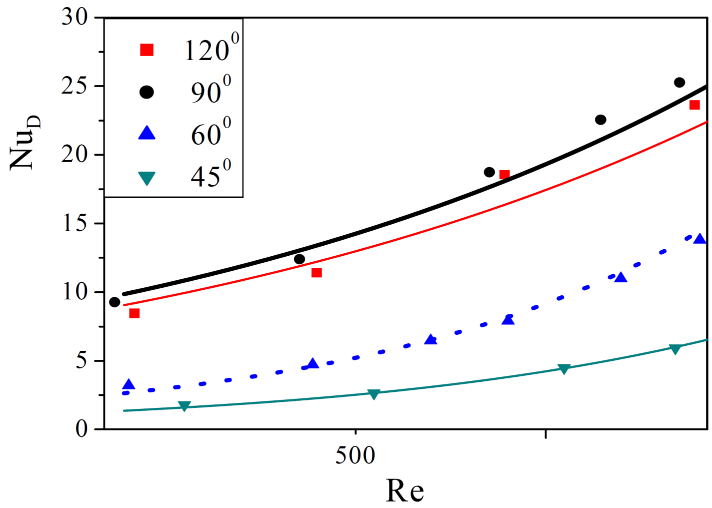


(b) $Nu_D$

**Figure 6 $f_D$ and $Nu_D$ of ducts with different included angles**

Comparing Fig 6 shows that the included angle has different effects on $f_D$ and $Nu_D$. The flow in the duck with α=90 has the largest friction factor and Nusselt number. Under the same Reynolds number, $f_D$ at α=120° is lower than $f_D$ at α=60° and 45°, whereas, $Nu_D$ at α=120° is higher than $Nu_D$ at α=60° and 45°. This difference indicates that the included angle influences the flow and heat transfer in cross-corrugated triangular ducts in different ways. However, it is difficult to explain this phenomenon with the mathematic model (Equ 1-7). Therefore, the field synergy principle was introduced to further explore the mechanism.

## 5 The effects of included angles on flow and heat transfer

### *5.1 Introduction to the field synergy principle*

To improve heat transfer performance, Guo et al. [7,8] proposed the principle of field synergy – the synergy of the velocity field and the temperature gradient field in the fluid domain. By introducing two dimensionless variables:

$$\overline{U} = \frac{U}{U_\infty}, \nabla\overline{T} = \frac{\nabla T}{(T_\infty - T_w)/\delta_t} \tag{15}$$

the energy equation of a steady, 2-D boundary layer flow over a cold flat plate at zero incident angle can be written as:

$$Nu_x = Re_x Pr \int_0^1 (\overline{U} \cdot \nabla\overline{T}) d\overline{y} \tag{16}$$

The vector dot product $\overline{U} \cdot \nabla\overline{T}$ in the dimensionless integration can be expressed as:

$$\overline{U} \cdot \nabla\overline{T} = |\overline{U}||\nabla\overline{T}| cos\beta \tag{17}$$

Where β is the included angle between the velocity vector and the temperature gradient (heat flow vector). Equ 17 shows that in the convection domain there are two vector fields, U and $\nabla T$, or three scalar fields, $|\overline{U}|$, $|\overline{\nabla T}|$ and cosβ. Hence, the value of the integration or the strength of the convection heat transfer depends not only on the velocity, the temperature gradient, but also on their synergy. The field synergy principle indicates that improving synergy for the velocity and temperature gradient/heat flow fields can markedly enhance heat transfer with less increased flow resistance.

### *5.2 Application of the field synergy principle*

The flow in the cross-corrugated triangular duct can be simplified to 2-dimension as well, as shown in Figure 7. According to the filed synergy principle, the energy equation can be written as:

$$\iint_{\Omega=abcdea} \rho c_p (\vec{U} \cdot \nabla T) dxdz - \int_{cd} \vec{n} \cdot k \nabla T ds - \int_{ea} \vec{n} \cdot k \nabla T ds = \int_{abc} \vec{n} \cdot k \nabla T ds + \int_{de} \vec{n} \cdot k \nabla T ds \qquad (18)$$

Where $\vec{n}$ is the surface unit normal vector and *s* is the arc length along boundary.

The first item on the left side of Equ. 18 presents the heat transfer caused by flow and the second and third items present the heat transfer by conductivity. The difference equals to the heat transfer by convection.

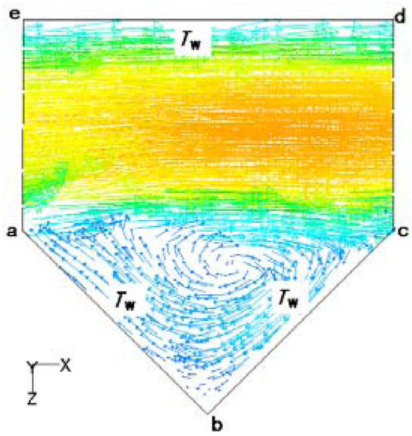


**Figure 7 Two dimensional flow field**

Since for the most cases of elliptic type convective heat transfer, the Peclet number is larger than 100, the transferred heat by conductivity can be ignored. Therefore, the integration (*Int*) of the left side of Equ. 18 can be written as:

$$Int = \int \rho c_p |\vec{U}| |\nabla T| \cos \beta ds \qquad (19)$$

### *5.3 Domain averaged included angle*

Based on Equ 18, the most efficient method to enhance the convective heat transfer is to reduce the angle β. To reveal the variation trend of the included angle between velocity and temperature gradient, a domain averaged included angle was defined as:

$$\beta_m = \sum \cos^{-1}\left(\frac{\vec{u}}{\left|\vec{u}\right|}\frac{grad(t)}{|grad(t)|}\right)\frac{\Delta V}{V} \tag{20}$$

$\beta_m$ was calculated for the flow in the cross-corrugated triangular ducts with different included angles. Results were displayed in Fig 8. Obviously, the flow in the cross-corrugated triangular duct with α=90 has the smallest domain averaged included angle, which implies the best synergy performance. Moreover, for a specified included angle (α), $\beta_m$ first rises and then drops along with the change of Reynolds number. There always exists an extreme value which normally appears in a Reynolds number range of 800-1200. At the extreme value of $\beta_m$, flow and heat transfer has the worst synergy performance. It shall also be pointed out that it is not necessary to have a small amount of heat transferred by convection or $Nu_m$ at big $\beta_m$, because the convection depends on the absolute value of velocity vector and the temperature gradient as well, according to Equ 17.

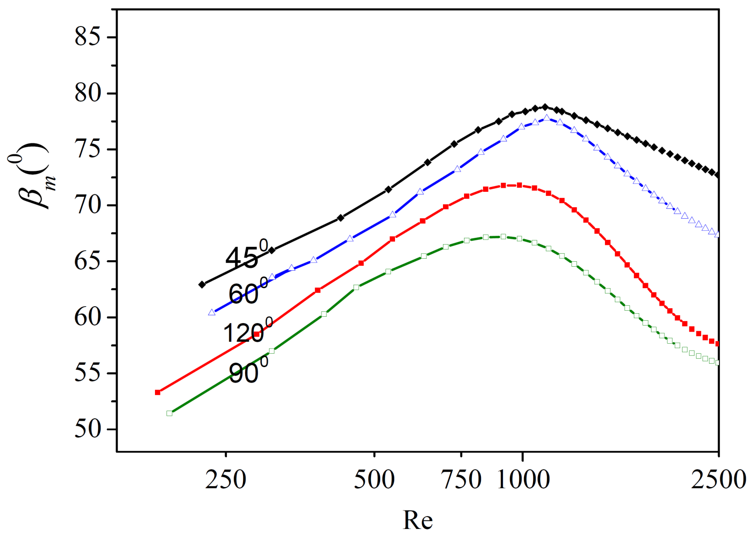


**Figure 8 $\beta_m$ of different flow channels**

***5.4 Validation of the field synergy principle***

To evaluate the performance of plate heat exchanger, a dimensionless performance evaluation criterion (PEC) was defined as [11]:

$$PEC = St \cdot \mathrm{Pr}^{2/3} / f_m \tag{21}$$

Where St is Stanton number.

Fig 9 shows the PEC of the cross-corrugated triangular ducts with different included angles. It is clear that the duck with α=90$^o$ has the highest PEC, which implies the best performance of heat transfer. This is consistent to the results of the field synergy principle.

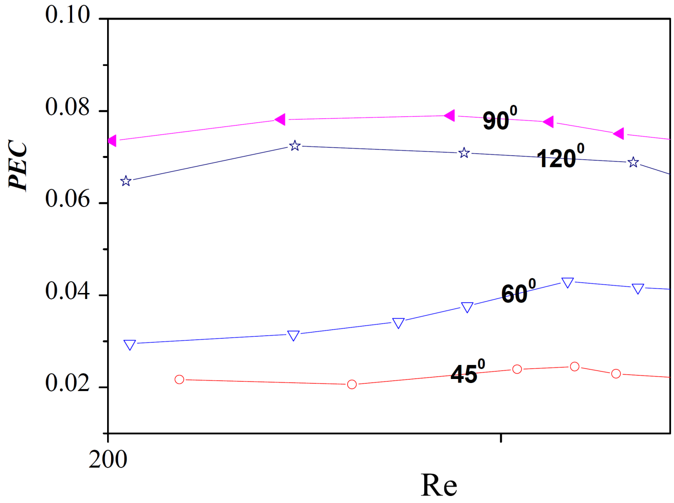


**Figure 9 PEC of ducts with different included angles**

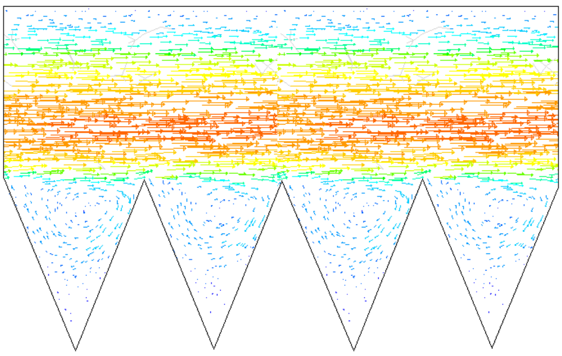

(a) α=45°

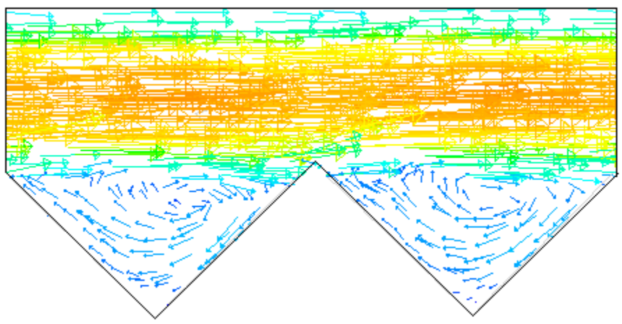

(b) α=90°

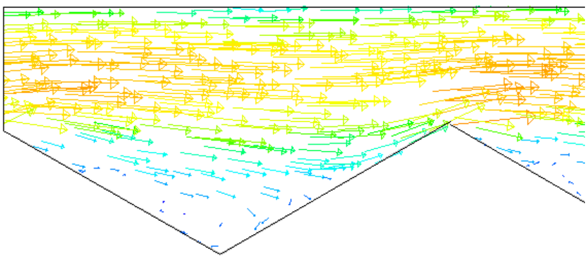

(c) α=120°

**Figure 10 Velocity vector at $y^*$=0.5 with different included angles**

In addition, the results of velocity vector and temperature distribution also support the conclusion of the field synergy principle. Fig 10 and 11 show the velocity vector and temperature distribution at $y^* = y/y_0 = 0.5$ with different included angles. It is easy to understand that the generated vortex in the lower part of the channel section can greatly improve the synergy between flow and heat transfer. Comparing the vortexes formed in different channels with different included angles, those in the channel with α=90 have the highest intensity and, consequently disturb the flow in the upper part of the channel. Therefore, the duck with α=90 has the best performance of heat transfer.

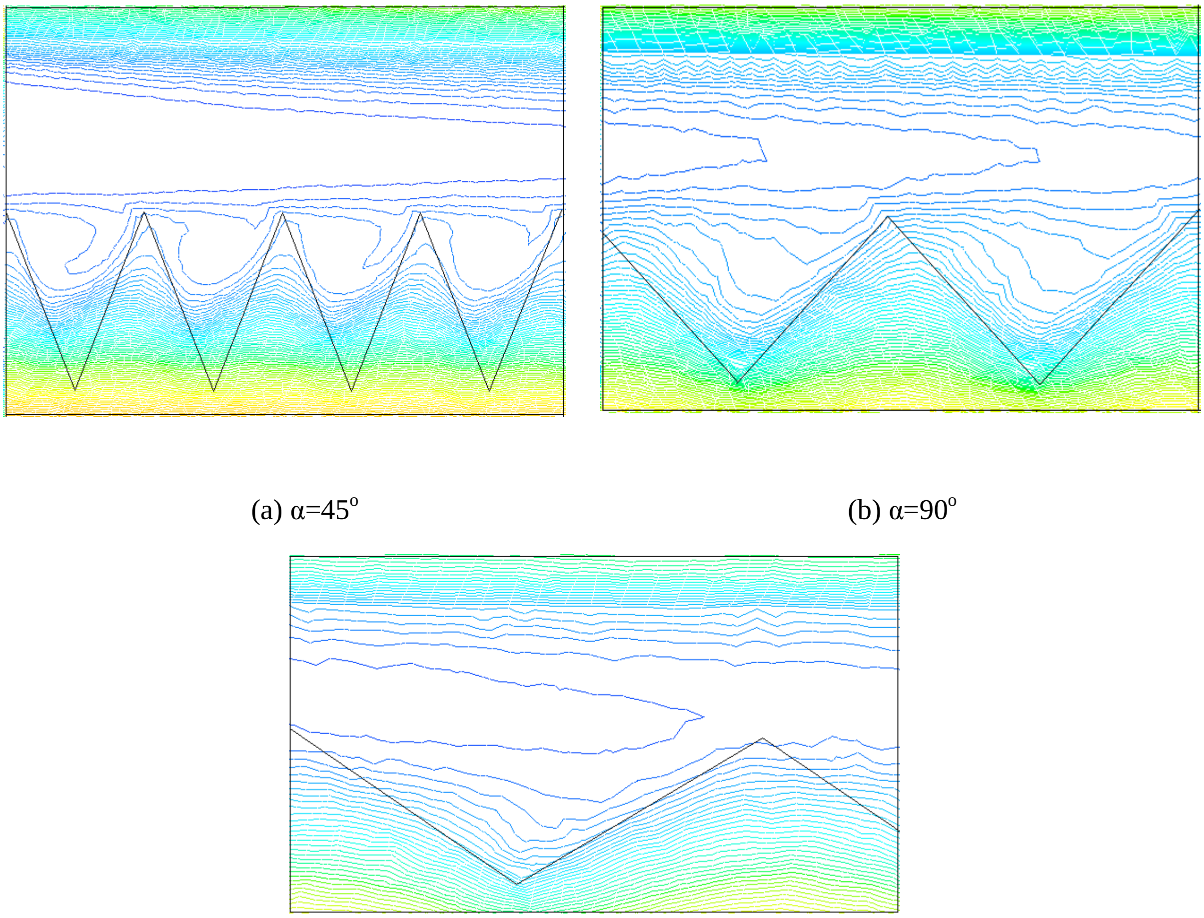

(a) $\alpha=45^o$ (b) $\alpha=90^o$

(c) $\alpha=120^o$

**Fig11 Temperature distribution at $y^*=0.5$ with different included angles**

## 6 Conclusions

The impacts of included angles on the fluid flow and convective heat transfer in cross-corrugated triangular ducts were investigated under uniform heat flux boundary conditions. The results about the friction factor and Nusselt number from both experiments and simulations show that the flow in the duck with $\alpha=90^o$ has the largest friction factor and Nusselt number. However, the included angle influences the flow and heat transfer in cross-corrugated triangular ducts in different ways. For example, under the same Reynolds number, $f_D$ at $\alpha=120^o$ is lower than $f_D$ at $\alpha=60^o$ and $45^o$, whereas, $Nu_D$ at $\alpha=120^o$ is higher than $Nu_D$ at $\alpha=60^o$ and $45^o$.

By introducing the field synergy principle, the different impacts of the included angle was further explored. Results show that the flow in the cross-corrugated triangular duct with $\alpha=90^o$ has the smallest domain averaged included angle ($\beta_m$), which implies the best synergy performance. In addition, there always exists an extreme value of $\beta_m$, which normally appears in a Reynolds number range of 800-1200. At the extreme value of $\beta_m$, flow and heat transfer has the worst synergy performance. The results of the field synergy principle were also validated by analyzing the performance evaluation criterion and studying the velocity vector and temperature distributions.

**Acknowledgment**
This project is supported by Natural Science Foundation of China (NSFC) No.51076047, and Specialized Research Fund for the Doctoral Program of Higher Education No. 20070561034.

**Nomenclature**

| | |
|---|---|
| $A_{ci}$ | cross-sectional area at inlet or outlet of a cycle ($m^2$) |
| $A_{cyc}$ | surface area of the channel ($m^2$) |
| $c_p$ | specific heat [kJ/(kgK)] |
| $D_h$ | hydraulic diameter of the channel (m) |
| $f$ | friction factor |
| $f_D$ | fully developed local or cyclic mean friction factor |
| $h$ | static enthalpy (kJ/kg); or heat transfer coefficient [kW/($m^2$K)] |
| $H$ | total enthalpy (kJ/kg) |
| $k$ | thermal conductivity [kW/(mK)] |
| $L_{cyc}$ | length of a cycle in flow direction (m) |
| Nu | Nusselt Numbers |
| $Nu_D$ | fully developed local or cyclic mean Nusselt numbers |
| $p$ | pressure (Pa) |
| Pr | Prandtl Numbers |
| Re | Reynolds number |
| St | Stanton number |
| $t$ | time (s) |
| $T$ | temperature (K) |
| $u$ | flow velocity (m/s) |
| $V_{cyc}$ | volume of channel ($m^3$) |
| $x$, $y$ or $z$ | coordinates (m) |
| $y_0$ | pitch of the repeated segment of the duct (m) |
| $z_0$ | width of the repeated segment of the duct (m) |

Greek letters

| | |
|---|---|
| $\rho$ | fluid density (kg/$m^3$) |
| $\mu$ | molecular viscosity (Ns/$m^2$) |

Superscripts

| | |
|---|---|
| * | dimensionless |

Subscripts

| | |
|---|---|
| D | Fully developed |
| i | inlet |
| L | local |
| m | mean |
| o | outlet |
| w | wall |

**References**

[1] Scott K. et al., Intensified membrane filtration with corrugated membranes, J. Membrane Sci. 173 (2000), pp. 1-16.
[2] Scott K., Lobato J., Mass transport in cross-corrugated membranes and the influence of TiO2 for separation processes, Ind. Eng. Chem. Res. 42 (2003), pp. 5697-5701.
[3] Zhang L.Z., Numerical study of periodically fully developed flow and heat transfer in cross-corrugated triangular channels in transitional flow regime, Numer. Heat Transfer A - Appl. 48 (2005), pp. 1-19.
[4] Zhang L.Z., Convective mass transport in cross-corrugated membrane exchangers, J. Membrane Sci. 260 (2005), pp. 75-83.
[5] Zhang L.Z., Heat and mass transfer in a total heat exchanger: cross-crrugated triangular ducts with composite supported liquid membrane, Numer. Heat Transfer A - Appl. 53 (2008), pp. 1195-1210.
[6] Zhang L.Z., Chen Z.Y., Convective heat transfer in cross-corrugated triangular ducts under uniform heat flux boundary conditions. Int. J. Heat Mass Transfer. 54 (2011), pp. 597-605.
[7] Guo Z.Y., Tao W.Q., Shah R.K., The field synergy (coordination) principle and its applications in enhancing single phase convective heat transfer, Int. J. Heat Mass Transfer. 48 (2005), pp. 1797-1807.
[8] Chen Q., Ren J.X., Guo Z.Y., Fluid flow field synergy principle and its application to drag reduction, Chinese Science Bulletin. 53 (2008), pp 1-5.
[9] Zhang L.Z., Turbulent three-dimensional air flow and heat transfer in a cross-corrugated triangular duct. ASME Journal of Heat Transfer, 127 (2005), 10, pp. 1151-1158.
[10] Fluent, ANSYS, Inc. 2011
[11] Leng X.L. et al., Methods for Applying Field Synergy Principle in Convection Heat Exchange. Journal of Engineering for Thermal Energy& Power, 124 (2009), 13, pp. 352~ 354 (in Chinese).